Modulation of mantle plumes and heat flow at the core mantle boundary by plate-scale flow: results from laboratory experiments

Helge M. Gonnermann[a],[*], A. Mark Jellinek[b],[1], Mark A. Richards[a],[2], Michael Manga[a],[3]

[a]*Department of Earth and Planetary Science, University of California, 307 McCone Hall, Berkeley, CA 94720-4767, USA*
[b]*Department of Physics, University of Toronto, 60 St. George St., Toronto ON, Canada M5S 1A7*

Abstract

We report results from analog laboratory experiments, in which a large-scale flow is imposed upon natural convection from a hot boundary layer at the base of a large tank of corn syrup. The experiments show that the subdivision of the convective flow into four regions provides a reasonable conceptual framework for interpreting the effects of large-scale flow on plumes. Region I includes the area of the hot thermal boundary layer (TBL) that is thinned by the large-scale flow, thereby suppressing plumes. Region II encompasses the critically unstable boundary layer where plumes form. Region III is the area above the boundary layer that is devoid of plumes. Region IV comprises the area of hot upwelling and plume conduits. Quantitative analysis of our experiments results in a scaling law for heat flux from the hot boundary and for the spatial extent of plume suppression. When applied to the Earth's core–mantle boundary (CMB), our results suggest that large-scale mantle flow, due to sinking lithospheric plates, can locally thin the TBL and suppress plume formation over large fractions of the CMB. Approximately 30% of heat flow from the core may be due to increased heat flux from plate-scale flow. Furthermore, CMB heat flux is non-uniformly distributed along the CMB, with large areas where heat flux is increased on average by a factor of 2. As a consequence, the convective flow pattern in the outer core may be affected by CMB heat-flux heterogeneity and sensitive to changes in plate-scale mantle flow. Because of plume suppression and 'focusing' of hot mantle from the CMB into zones of upwelling flow, plume conduits (hotspots) are expected to be spatially associated with lower-mantle regions of low seismic velocities, inferred as hot upwelling mantle flow.
© 2004 Elsevier B.V. All rights reserved.

Keywords: mantle convection; plumes; hotspots; thermal boundary layer; core–mantle boundary; core heat flow; thermal convection

* Corresponding author. Tel.: +1 510 643 8328; fax: +1 510 643 9980.
E-mail addresses: hmg@seismo.berkeley.edu (H.M. Gonnermann), markj@physics.utoronto.ca (A.M. Jellinek), markr@seismo.berkeley.edu (M.A. Richards), manga@seismo.berkeley.edu (M. Manga).
[1] Tel.: +1 416 946 8130; fax: +1 416 978 7606.
[2] Tel.: +1 510 642 8560; fax: +1 510 643 9980.
[3] Tel.: +1 510 643 8532; fax: +1 510 643 9980.

1. Introduction

Heat flow from the Earth's core determines the growth of the inner core, affects geodynamo energetics and contributes to the secular cooling of the Earth. Core heat flow is poorly known and estimates range from 2 TW to 10 TW [1]. Lower-bound estimates come from plume buoyancy flux calculations [2,3], assuming that they represent the total heat flux from the core–mantle boundary (CMB). At the Earth's surface, major intraplate volcanic hotspots, such as Hawaii, for example, are generally attributed to mantle plumes arising from the core–mantle boundary. However, mantle plumes are thought to be of secondary importance relative to plate-scale convective flow associated with plate motions and subduction [2,4]. Hence, one might expect great difficulty in attempting to interpret, e.g., the distribution and fluxes of hotspots in terms of core–mantle boundary processes.

Plate-scale flow will affect plume dynamics in at least two fundamental ways: (1) plumes will be advected in the large-scale flow associated with plate motions [5–10], and (2) the formation of mantle plumes at the core–mantle boundary will be modulated by thinning and thickening of the boundary layer due to large-scale flow and the impingement of cold downwelling slab material [11,12]. Consequently, any inference of mantle dynamics or core heat flow, based on the spatial distribution and buoyancy fluxes of hotspots, requires an improved understanding of the interactions between plate-scale mantle flow, the formation of plumes at the CMB, and their ascent through the Earth's mantle.

Another important aspect of plate-scale mantle flow derives from the fact that it is much slower than convection in the outer core (by approximately a factor of 10^9) and hence it is expected to induce long-term lateral variability of CMB heat flux due to variations in thermal gradients at the CMB [11–15]. It has been inferred that such spatial heterogeneity in CMB heat flux affects the structure (e.g., [16]) and reversal pattern (e.g., [17,18]) of the Earth's magnetic field, presumably through modulation of the convective flow of the Earth's outer core [15,19–22].

Although advection of plumes in the plate-scale mantle flow has been studied in some detail [5–10,12], the effect of non-turbulent, large-scale flow in modulating instabilities at a hot boundary layer has received relatively little attention. The latter is a significant challenge since three-dimensional numerical convection models are still limited in their ability to simulate both plate-scale mantle flow and plume-scale thermal convection from a hot thermal boundary layer, especially in the presence of temperature-dependent mantle viscosity [23–25].

The purpose of this study is to provide insight into the effect of plate-scale mantle flow on heat flux and the modulation of plume formation at the CMB. In a previous paper [12], we described exploratory experiments in which a large-scale flow was imposed upon natural convection from a hot boundary layer at the base of a large tank of corn syrup. A number of useful insights resulted from this work. There are relatively well-defined transitions in convection from the hot boundary, ranging from plume-dominated heat flux and flow, to complete capture of the hot boundary layer by the imposed large-scale flow. Here we extend this work with more detailed experiments at *Ra* between 10^6 and 10^8, leading to a more quantitative understanding of how plate-scale flow modulates thermal instabilities and heat flux from a hot boundary layer (Sections 4 and 5).

We apply these results to show (1) how the interaction between plume- and plate-scale mantle flow may affect the geographic distribution of hotspots (Section 6.1) and (2) why hotspots seem to be associated with slow seismic velocities in the lower mantle (Section 6.2). Furthermore, we present a scaling law that quantifies (3) the fraction of core heat flow associated with plate-scale mantle flow (Section 6.3), as well as (4) the lateral heterogeneity in CMB heat flux (Section 6.4).

2. Experimental setup

Our convection experiments (see [12] for additional details about the experimental setup) are conducted in a large ($1.5 \times 1.5 \times 0.6$ m deep) tank that is filled with corn syrup (Fig. 1). The viscosity of the corn syrup decreases strongly with increasing temperature [12]. The sidewalls are glass, insulated with 20 cm of styrofoam insulation. The bottom of the tank is heated and consists of an aluminum heat exchanger through which hot water is circulated, so that the
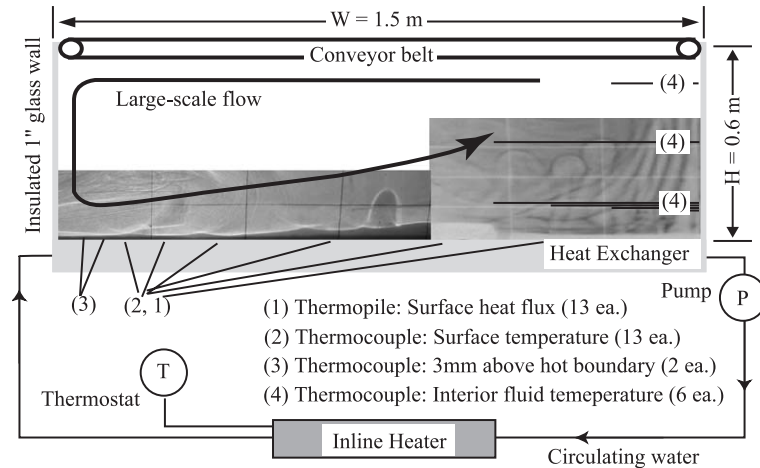
Fig. 1. Schematic diagram of experimental setup.

lower boundary condition is isothermal [12]. Immersed in the syrup, at the top of the tank, is a conveyor belt used to generate a large-scale recirculating flow. We measure heat flux and temperature at the hot boundary using an array of Omega HFS-4 thermopile sensors. These sensors are arranged so that we obtain measurements at 15 cm intervals along the large-scale flow direction. In addition, thermocouples are installed at the sidewalls and the tank interior, providing estimates of sidewall heat loss and vertical temperature profiles in the fluid interior. In each experiment, comparison of shadowgraph images of the fluid motions indicates that the sensors have no significant influence on the flow.

Prior to the start of our experiments, the syrup is brought to equilibrium at room temperature. During the experiment, hot water at constant temperature is recirculated through the bottom heat exchanger at a high rate from an in-line heater. After a short time period during which the water temperature rises to the prescribed value, the temperature at the bottom boundary remains constant. The duration of this time period is much less than the initial transient period associated with growth of the hot TBL. No data from this initial period is used for our analysis. Because there is no cooling at the top of the tank, the internal temperature of the syrup increases during the course of an experiment. Consequently, syrup viscosity decreases and Rayleigh number increases with time. These changes occur on a time scale that is long compared with the time scale for plume formation, so

that quasi-steady-state flow conditions are achieved [12].

3. Experimental parameters

For a Newtonian fluid, the dynamical state of convection is governed by the Rayleigh number, $Ra=\rho g\alpha\Delta TH^3/(\mu_a\kappa)$, a measure of convective vigor, and the Prandtl number, $Pr=\mu_a/(\rho\kappa)$. Here g is the gravitational acceleration, α is the coefficient of thermal expansion, ΔT is the temperature difference between hot boundary and fluid interior, μ_a is the viscosity at the average interior temperature, ρ is the density, κ is the thermal diffusivity, and H is the characteristic length scale (depth of fluid). In all of our experiments the Prandtl number is large ($>10^4$) so that the characteristic viscous time scale is much shorter than the time scale for thermal diffusion. Furthermore, the influence of inertial forces is negligible, because the Reynolds number, $Re=UH\rho/\mu_a<1$ (here U is the characteristic horizontal large-scale velocity, see Table 1 for a summary of the symbols and parameters). Consequently, our experiments are distinct from analogous work in the turbulence community (e.g., [26]). Because of the strong temperature dependence of viscosity, thermal and velocity boundary layers are approximately of similar thickness. The ratio, γ, of the interior fluid viscosity to the viscosity of fluid at the hot boundary is $10\leq\gamma\leq100$ for all the data presented in this paper. Hence, the flow above the hot boundary

Table 1
Symbols and parameters

Symbol	Value/unit	Parameter
k	W m^{-1} $^{\circ}$C^{-1}	thermal conductivity (see [12] for more details)
$q(x)$	W m^{-2}	heat flux
q_I	W m^{-2}	heat flux for Region I, $q_\mathrm{I}{=}f(x)$
$\bar{q}_\mathrm{I}$	W m^{-2}	spatially averaged heat flux for Region I
q_II	W m^{-2}	heat flux for Region II, $q_\mathrm{II}{\neq}f(x)$
q_c	W m^{-2}	heat flux across critically unstable TBL, $q_\mathrm{c}\approx q_\mathrm{II}$
q_k	W m^{-2}	hypothetical conductive heat flux, $q_k{=}k\Delta T/H$
x	m	horizontal coordinate
A_I	m^2	area covered by Region I
A_II	m^2	area covered by Region II
A_CMB	1.5271×10^{14} m^2	surface area of the Earth's core
C	2.4 ± 0.6	empirical constant
D	m	lateral extent of Region I (Eq. (8))
H	0.6 m	characteristic length scale (depth of fluid layer)
Q	W	heat flow
Q^*	$Q_\mathrm{Region\ I}/Q_\mathrm{total}$	magnitude of heat-flux heterogeneity
R_core	3.486×10^6 m	radius of Earth's core
ΔT	$^{\circ}$C	temperature difference across TBL
U	m s^{-1}	characteristic horizontal velocity
U_m	cm year^{-1}	velocity of plate-scale mantle flow in lowermost mantle
α	5.61×10^{-4} $^{\circ}$C^{-1}	coefficient of thermal expansion (see [12] for more details)
β	0.33 ± 0.01	empirical exponent for $Nu\sim Ra$ relation
δ	m	thickness of TBL
δ_c	m	thickness of critically unstable TBL
γ	$\mu_\mathrm{a}/\mu_\mathrm{tbl}$	viscosity ratio
κ	10^{-7} m^2 s^{-1}	thermal diffusivity
μ_a	Pa s	viscosity of ambient fluid above TBL[a]
μ_tbl	Pa s	viscosity of fluid at the hot boundary[a]
Nu	$q/q_k\sim Ra^{\beta}$	Nusselt number
Pe	UH/κ	Peclet number
Pr	$\mu_\mathrm{a}/\rho\kappa$	Prandtl number
Ra	$g\rho\alpha_\mathrm{c}\Delta TH^3/\mu_\mathrm{a}\kappa$	Rayleigh number
Re	$UH\rho/\mu_\mathrm{a}$	Reynolds number

[a] The viscosity of the ADM 62/44 corn syrup used in these experiments varied with temperature T ($^{\circ}$C) according to $\mu(T){=}\exp(15.92{-}0.19\,T{+}0.00078T^2)$ mPa s.

experiences very low drag from the boundary and can be treated as having an approximately free-slip lower boundary [12].

The coupled large- and plume-scale convective flow is characterized by two externally controlled parameters: (1) the Rayleigh number and (2) the Peclet number, $Pe{=}UH/\kappa$, a non-dimensional representation of the imposed large-scale flow velocity. Ra varies between approximately 10^6 and 10^8 during each experiment. As Ra increases, the characteristic plume size and rise time decrease, while the number of plumes and their frequency of generation increase.

These parameter ranges represent reasonable lower and upper bounds that are applicable to the Earth's core–mantle boundary region. Although whole-mantle convection may be characterized by Rayleigh numbers as high as 10^8–10^9, the viscosity of the lower mantle is probably one to two orders of magnitude higher than that of the upper mantle [27–30], so the range ($10^6{\leq}Ra{\leq}10^8$) appears appropriate. The range of imposed velocity U (or, alternatively, Pe) used in our experiments span the range of behavior of interest, i.e., from plume-dominated flow ($U{=}0$, $Pe{=}0$) to complete suppression of plumes for higher U and Pe. The large-scale flow imposed in the laboratory experiments corresponds to flow velocities in the lowermost mantle as large as approximately 4 cm/yr.

4. Qualitative results

In the absence of large-scale flow ($Pe{=}0$) convection is dominated by upwelling plumes (Fig. 2a). Because velocity and thermal boundary layers are of similar thickness, at $Pe{>}0$ large-scale flow may advect hot TBL fluid laterally (x-direction) along the heated bottom at a faster rate than conductive growth of the TBL. As a consequence, the TBL may be locally thinned to subcritical thickness, with plumes being suppressed along part of the TBL (Figs. 2b and 3). The TBL is thinnest in the vicinity of the downwelling flow (small x) and grows in thickness in the flow direction (increasing x). At some critical distance from the downwelling ($x{=}D$), advective thinning of the TBL is balanced by conductive growth and plumes form at $x{\geq}D$. Thus, at sufficiently large values of Pe, plumes are
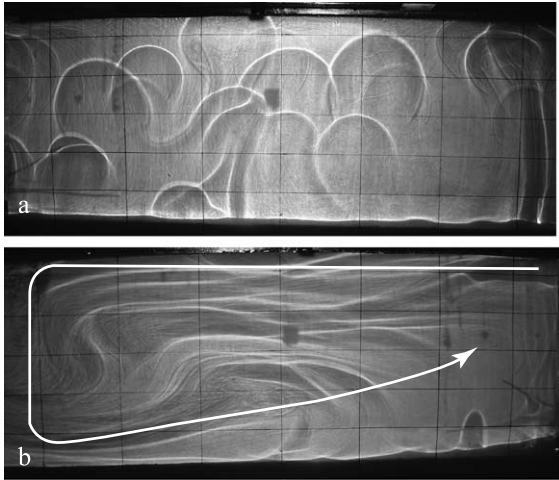
Fig. 2. (a) Shadowgraph at $Ra \approx 1 \times 10^6$, $Pe=0$, $\gamma \approx 100$. Grid dimension is 20×10 cm. (b) Shadowgraph at $Ra \approx 5 \times 10^6$, $Pe \approx 1 \times 10^4$, $\gamma \approx 100$. Note the increasing thickness of the thermal boundary layer in the downstream direction.

suppressed throughout the entire tank. At intermediate values of Pe, plumes are only suppressed along part of the hot bottom boundary.

Determining how D varies with Ra and Pe is one of the main goals of our experiments. Above the TBL at $x \geq D$ rising plumes are advected laterally by the large-scale flow toward the upwelling. In the area of upwelling flow, horizontal velocities decrease and the rate at which plumes and conduits are advected laterally decreases. It is conceptually useful to subdivide the convective flow associated with high Rayleigh number mixed convection (i.e., thermal convection plus forced flow) into four distinct regions (Fig. 4).
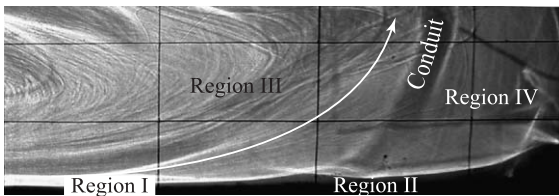

Fig. 3. Shadowgraph of plume conduit. Area of photograph represents the bottom right-hand corner of Fig. 2b, but at a later time. The bottom of the conduit is located near the edge of Region II (note the thickened TBL at the base of the conduit). $Ra \approx 4 \times 10^6$, $Pe \approx 1 \times 10^4$, $\gamma \approx 100$.
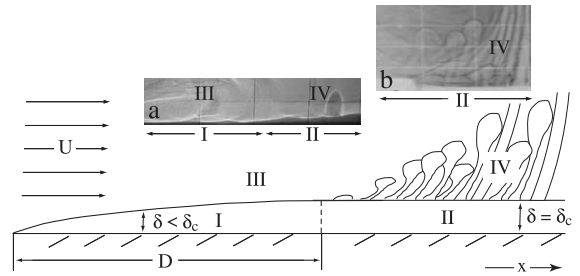

Fig. 4. Schematic diagram depicting the four convective regions. Photo inserts are shadowgraph images of the actual flow structures associated with these Regions. The leftmost three quarter of insert (a) depicts Regions I and III, where the TBL is subcritical. Note the absence of plumes and thickening of the TBL in the downstream direction (toward the right). The rightmost quarter of insert (a) shows the formation and rise of a single plume. In contrast, insert (b) depicts the plumes and plume conduits associated with Regions II and IV.

4.1. Region I

Region I represents the subcritical TBL $(x<D)$. In this area, the TBL is thinned to subcritical thickness by the large-scale flow and instabilities of the TBL resulting in the formation of plumes are suppressed. Heat flux is inversely proportional to TBL thickness, δ. Hence, for a constant temperature boundary condition, heat flux in Region I, q_I, is increased relative to a control case with $Pe=0$ and otherwise identical conditions (e.g., Ra). Because δ increases with increasing x, q_I will also decrease with x.

4.2. Region II

Region II represents the critically unstable TBL $(x \geq D)$. This is the zone of plume formation where, on average, the TBL is of critical thickness, δ_c. In this region, the time-averaged vertical heat flux, q_{II}, is spatially uniform and approximately equal to heat flux at $Pe=0$. In addition to generating new plumes, Region II represents the 'root zone' of plume conduits (Fig. 3).

4.3. Region III

Region III is the area above the TBL that is devoid of plumes. This region is dominated by the imposed large-scale flow and encompasses the entire volume of

fluid above Region I. It also includes an area above Region II, where ascending plumes have been advected downstream by the large-scale flow. The temperature of the fluid comprising this region is relatively uniform and unaffected by the underlying TBL. Note that there are no cold downwelling structures in these experiments.

4.4. Region IV

Region IV comprises that area above Region II where ascending plumes and plume conduits are present (Fig. 3). Region IV includes the buoyancy flux from both Regions I and II. Plume conduits were observed to remain active over at least one plume-rise time, with some remaining active longer. During their lifetime, plume conduits do not remain stationary. However, because conduits are located within the zone of upward flow where horizontal velocities are small, their lateral mobility is small when compared to the induced large-scale flow. Finally, owing to the combined buoyancy flux from Regions I and II, the spatially averaged temperature of Region IV is higher than for Region III or for experiments at similar Ra, but $Pe=0$.

5. Theoretical scaling for heat flux and quantitative experimental results

5.1. Scaling theory

Based on boundary layer theory it is possible to derive scaling laws [12,31–34] for the thickness of the TBL, $\delta(x)$, and heat flux, $q(x)$, during thermal convection with an imposed velocity, U. In our experiments, we measure heat flux at the bottom boundary directly, allowing us to calibrate the scalings derived below.

We seek scalings for $\delta(x)$ and $q(x)$ in Region I, the area over which plume instabilities are suppressed by the large-scale flow (as shown in Section 5.2, within Region II heat flow is little-affected by the large-scale flow.) Our analysis is based on the assumption that the bottom boundary can be approximated as free-slip [12] for suitably large ratios of viscosity between ambient and hot TBL fluid, i.e., $\gamma \geq 10$. Balance between conduction of heat from the hot boundary

and lateral advection of heat induced by flow within the TBL gives [12]

$$U \frac{\Delta T}{x} \sim \kappa \frac{\Delta T}{\delta^2}, \tag{1}$$

or

$$\delta(x) \sim \sqrt{\frac{x\kappa}{U}} = \sqrt{\frac{Hx}{Pe}}, \tag{2}$$

where $\sim$ means "approximately equal to," κ is thermal diffusivity, ΔT is the temperature difference between the hot boundary and ambient fluid, and H is the characteristic length scale (depth of fluid layer). Locally, heat flux across the TBL is given by Fourier's law

$$q(x) \sim k\Delta T/\delta(x), \tag{3}$$

In the absence of large-scale flow ($Pe=0$), heat flux across the convecting fluid layer is given by

$$q_c \sim k\Delta T/\delta_c, \tag{4}$$

where δ_c is the critical TBL thickness. Note that both q_c and δ_c are independent of x. Using the Nusselt number, Nu, it is possible to derive a scaling for δ_c. The Nusselt number is a non-dimensional measure of the efficiency of the heat transfer process. It is determined by the ratio of measured heat flux across a thermally convecting layer of fluid, q_c, to the hypothetical conductive heat flux, $q=k\Delta T/H$, and is given by

$$Nu = \frac{q_c}{q} \sim \frac{H}{\delta_c}. \tag{5}$$

A well-established parameterization for Nu is given by $Nu \sim Ra^{\beta}$, e.g., [35,36], which in combination with Eq. (5) results in

$$\delta_c \sim HRa^{-\beta}. \tag{6}$$

Note, even though we have ignored the usual multiplicative constant in Eq. (6), it will implicitly be included via the empirical constant obtained from our subsequent scaling analysis. It is now possible to

estimate the ratio of the measured heat flux $q(x)$ at $Pe>0$ (Eq. (3)) to the measured heat flux from a control experiment at $Pe=0$ (Eq. (4)), by using Eqs. (2) and (6) to give

$$\frac{\delta_c}{\delta(x)} \sim \frac{q(x)}{q_c} = C(HPe/x)^{1/2}Ra^{-\beta}. \quad (7)$$

Here C and β are empirical constants that we seek to determine experimentally via heat-flux measurements. C is expected to be of order unity and, based on extensive previous work ([35,37] and references therein), β is expected to be approximately 1/3. Verifying and calibrating the behavior predicted in Eq. (7) is a primary goal of the experiments presented below.

For all experimental data included in our analysis ($10 \leq \gamma \leq 100$), the free-slip scaling of Eq. (7) provides an adequate approximation for these experiments [12,32,33]. Furthermore, a free-slip scaling is appropriate for application of our results to the Earth's CMB. We will demonstrate in the subsequent section that this scaling provides a good fit to our experimental data.

Finally, using Eq. (7) evaluated at $\delta(x)=\delta_c$, it is possible to estimate the distance from the downwelling over which plumes are suppressed (also an experimentally observable quantity)

$$D = C^2 HPeRa^{-2\beta}. \quad (8)$$

It should be pointed out that Eqs. (7) and (8) are not valid in the limit $x \rightarrow 0$, because of the finite width of downwelling flow.

5.2. Results

Fig. 5 shows data from one typical experiment at $Pe=1.5\times10^4$. All experimental data (temperature and heat flux) were collected at a frequency of approximately 0.3 Hz and resampled at approximately 0.1 Hz for ease of plotting. We analyzed data from four individual experiments. The average duration of a single experiment was approximately 10–20 h. However, only data after the transient start-up period (approximately 2–3 h) and with $\gamma \geq 10$ were included in our analysis.

Fig. 5 shows results from one experiment. Temperature data from two thermocouples are shown in Fig.
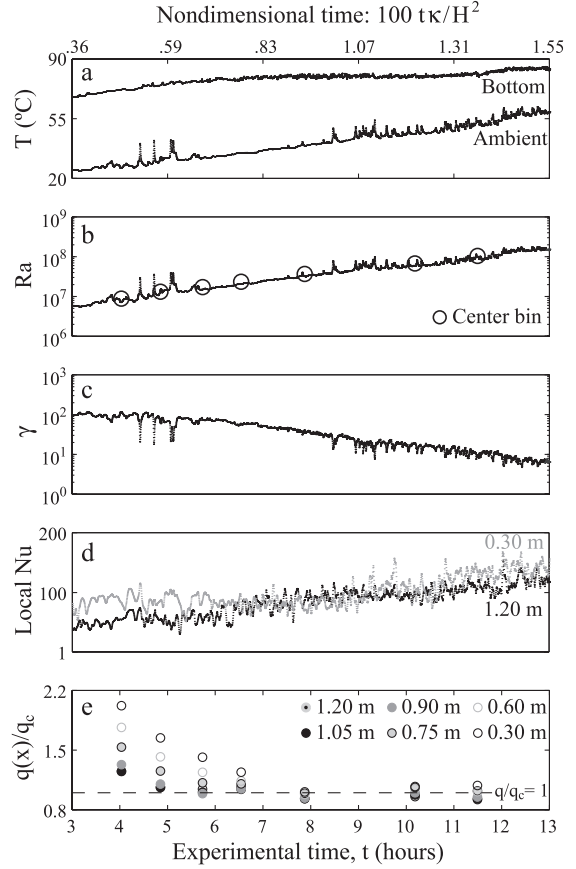
Fig. 5. Data from a typical experiment ($Pe=1.5\times10^4$). Horizontal axis is experimental time (t), or experimental time normalized by characteristic diffusion time ($100t\kappa/H^2$). (a) Temperature data from two select thermocouples for the heated bottom surface of the tank (i.e. TBL) and for ambient fluid approximately 10 cm above the TBL. Ambient fluid temperature is measured at several locations (Regions III and IV), but shown here is data from a thermocouple located within Region IV. The higher than average temperature spikes are due to the passage of plume heads or conduits near the thermocouple. (b) Ra based on temperature difference shown in (a). (c) Ratio of viscosity between ambient and hot TBL fluid, γ. (d) Local Nu for two different heat-flux sensors, $Nu(x)=q(x)/q_c$, where q_c is the heat flux from a control experiment with $Pe=0$. One sensor is located $x=0.3$ m and the other $x=1.2$ m from the downwelling sidewall. Note the difference in heat flux at early times. (e) Binned values for heat-flux ratio, q/q_c, at the bottom of the tank from six different positions along the direction of large-scale flow.

5a. High temperatures are measured at the bottom of the TBL, while the low-temperature data shown here are measured in the ambient fluid of Region IV. Actual temperatures used for Ra and γ during

calibration of scaling laws are average temperatures over all bottom thermocouples (Regions I and II) and all ambient thermocouples (Regions III and IV) for each experiment. The values of Ra (Fig. 5b) and γ (Fig. 5c) shown here are, however, based on the actual temperature data of Fig. 5a. All heat-flux data were binned by Ra at values indicated by the open circles in Fig. 5b, while $\gamma \geq 10$ for the considered range of Ra from this experiment (Fig. 5c). Fig. 5d shows how the imposed large-scale flow increases heat flux locally, as indicated by the local Nusselt number defined as $Nu(x) \sim q(x)H/(k\Delta T)$, where ΔT is the difference in temperature between ambient fluid and the heated bottom.

We also calculate the ratio between measured heat flux at a given location (i.e., a given heat-flux sensor), $q(x)$, to the measured heat flux, q_c, at equivalent Ra from the control experiment at $Pe=0$. Fig. 5e shows $q(x)/q_c$ for six different locations and for seven different times (or equivalently Ra) during the experiment. At low Ra, $q(x)$ is larger than q_c by up to a factor of 2 for the sensor located closest to the downwelling flow (smallest x). For a given Ra, $q(x)$ decreases with increasing downstream distance, x, until $q(x)/q_c \approx 1$ at $x \geq D$. Similarly, for a given Pe, as the value of D decreases with increasing Ra and $q(x)/q_c$ eventually reaches an approximately constant value of 1 at all locations (Fig. 5e). It should be noted that Eq. (7) is only applicable for $x \leq D$, or equivalently $q(x)/q_c \geq 1$.

Fig. 6 shows the fit for all experiments between measured heat-flux ratios and $q(x)/q_c$ predicted from Eq. (7). The data represent a range of Ra ($7 \times 10^6 < Ra < 2 \times 10^8$), Pe ($1.5 \times 10^4 < Pe < 3.6 \times 10^4$) and viscosity ratios, ($10 \leq \gamma \leq 100$). The characteristic time scale for the TBL to reach critical thickness, and hence the period of plume generation, decreases with increasing Ra. At the same time, the ratio between plume-rise velocity and the induced large-scale velocity, U, increases. Because of this secular change in conditions during the course of each experiment, Fig. 6 represents a broad range of convective dynamics [12]. Since $D \propto Ra^{-1}$, we find that for large-scale flow to noticeably affect heat-flux over the spatial dimensions and Ra range of our experiments (under the constraint that $\gamma \geq 10$), Pe must be $>10^3$. We therefore present experimental results in the range $Pe \sim 10^4$ in addition to $Pe=0$.
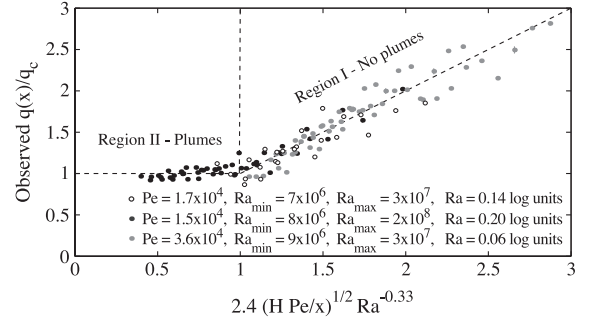

Fig. 6. Observed vs. predicted heat-flux ratio, $q(x)/q_c$, from three different experiments. Each experiment spans a range of Ra with viscosity ratios, $\gamma \geq 10$. Each data point represents one of six different heat-flux sensors located along the bottom of the tank and is averaged over an incremental range of Rayleigh number (see Fig. 5). Observed values of $q(x)$ represent measured heat flux at the bottom of the tank for a given Ra, Pe and position x, while q_c is the measured heat flux at the same Ra but for a control experiment with $Pe=0$. Error bars on individual data points (mostly the size of the data symbols and therefore hardly noticeable) represent the 99% confidence interval.

Each data point of Fig. 6 represents the Ra-binned heat flux for one Pe and one position, x. We only include measurements sufficiently far from the side-walls (0.3 m), so that boundary effects (i.e., variations in U) are small enough to be neglected. The average ambient fluid temperature, and hence viscosity, continuously change during the course of a single experiment (Fig. 5a). However, over the duration of several periods of plume generation these values vary only slightly [12], so that for each data point Ra varies by less than 0.20 log units.

As predicted from the analysis of the previous sections, there are two distinct regions of behavior evident in Fig. 6. On the left-hand side, the observed heat fluxes plateau at $q(x)/q_c \approx 1.0$, representing critical boundary layer behavior (Region II) and hence plume formation. Eq. (7) only applies to Region I, i.e., $q(x)/q_c \geq 1$, representing the part of the TBL over which plume instabilities are suppressed. We have found no pattern in the considerable scatter in the data. Instead, the scatter appears consistent with uncertainties (especially temporal variations) in the heat-flux measurements. We obtain $C=2.4 \pm 0.6$ and $\beta=0.33 \pm 0.01$, from a least-squares fit to the data shown in Fig. 6. The preliminary data from [12] permitted $0.28 < \beta \leq 0.33$ based on several experiments at $Pe=0$. The values reported here are approximately

consistent with other experimentally derived scalings, e.g., [12,37–41].

6. Applications to the Earth

The distribution of hotspots at the Earth's surface is used to infer dynamic processes occurring within the mantle [8–10,42–46]. Fig. 7 is a cartoon representation of the Earth's mantle illustrating common features of such interpretations (for more detailed discussions of lower-mantle structure, see [47,48] and references therein). Seismic tomography suggests that lithospheric plates sink into the lower mantle, e.g., [29,49,50], and references therein], driving plate-scale mantle flow [2,4,49,51]. The resultant cooling of the interior of the mantle is expected to increase the viscosity ratio between ambient and hot mantle at the CMB to $\gamma \geq 100$ [48,52,53]. As a consequence, all four convective regions described in Section 4 may occur within the Earth.

The main quantitative results of our work are given in Fig. 6, where the predictability of these regimes according to Eqs. (7) and (8) is demonstrated. In this section, we briefly discuss applications of these quantitative results to show that the qualitative view depicted in Fig. 7 is indeed a reasonable representation for the Earth's mantle. Specifically, we show to what extent plate-scale mantle flow (1) may affect the suppression of plumes over parts of the CMB, (2) may lead to lower-mantle regions with hotter than average temperatures and large buoyancy flux, (3) may account for approximately 30% of the total core heat flow, and (4) can generate spatial variability in CMB heat flux.

6.1. Plume suppression: Region I

In order to evaluate the affect of plate-scale mantle flow on the formation of plumes at the CMB we shall assume the following: (1) a Cartesian geometry; (2) a horizontal plate-scale flow in the
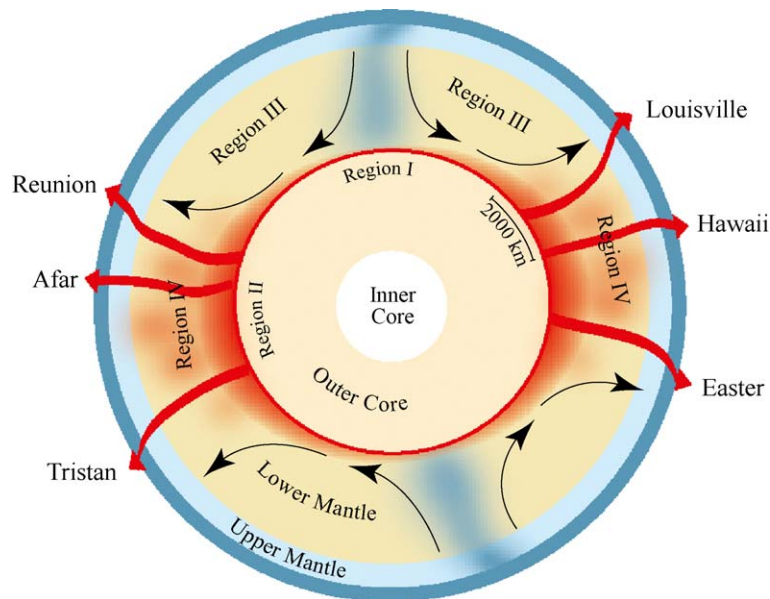

Fig. 7. Cartoon representation of an near-equatorial cross-section through the Earth based on the results of our experiments. Plate-scale flow (with lower-mantle velocity, U_m) is induced by sinking slabs. Plumes are expected to form above the CMB where the thermal boundary layer is critically unstable, denoted as Region II. Advective thinning of thermal boundary layer on both sides of the downwelling flow suppresses plume instabilities (Region I). Region III is dominated by plate-scale mantle flow and is devoid of plumes. Region IV is dominated by upward mantle flow. Plume conduits are located within and at the perimeter of Region IV. The conduits are relatively stationary, compared to plate velocities, because horizontal velocities are small in this area. Spatially averaged temperatures in Region IV are higher than those of Region III. Region IV may therefore be representative of seismic anomalies beneath Africa and the Pacific [54,58–63].

lowermost mantle with a width equivalent to half the circumference of the Earth's core; and (3) a velocity of $U_m \leq 2$ cm/year ($Pe \leq 10^3$), in accord with estimates for plate-scale lower-mantle velocities, e.g., [8,29]. It should be noted that this analysis, while simplified, is nonetheless consistent with the overall extent and magnitude of plate-scale flow in the lower mantle, e.g., [29,54].

Under these assumptions, and using Eq. (8), it is possible to estimate the areal extent of plume suppression, A_I, relative to the total surface area of the Earth's core, A_{CMB}, as

$$\frac{A_I}{A_{CMB}} = \frac{4\pi R_{core} D}{4\pi R_{core}^2} = \frac{D}{R_{core}}, \qquad (9)$$

where R_{core} is the radius of the Earth's core and the implicit factor of 2 is due to the fact that plume suppression is expected on both sides of the downwelling flow. The ratio A_I/A_{CMB} is shown in Fig. 8a as a function of assumed plate-scale velocity, U_m, and lower-mantle Rayleigh number (or equivalently viscosity). Most, if not all, hotspots appear to be distribution over approximately half of the Earth's surface, e.g., [46,55,56]. If projected onto the CMB, this implies that plumes are suppressed over approximately half the CMB. The parameter range (Ra and U_m) with plume suppression over $50 \pm 25\%$ of the CMB is shown as the gray shaded region in Fig. 8. Within the limitations posed by our analysis, we conclude that a value of the order of $Ra \sim 10^6$ ($\mu_a \sim 10^{22}$ Pa s) represents a reasonable estimate for an effective lower-mantle Rayleigh number. Based on the results of Fig. 8a, it appears unlikely that this value could be significantly larger than 10^6. Because the distance over which plumes are suppressed scales linearly with U_m, the distribution of hotspots is expected to be sensitive to global subduction rates, geometry, and history.

6.2. Hotspot location, large-scale seismic mantle structure: Regions III and IV

As a consequence of plume suppression (Region I) and lateral advection of plumes and conduits, plumes should occur predominantly in zones of upward large-scale flow (Region IV). This is apparently the case for Earth's hotspots [46,55,56],
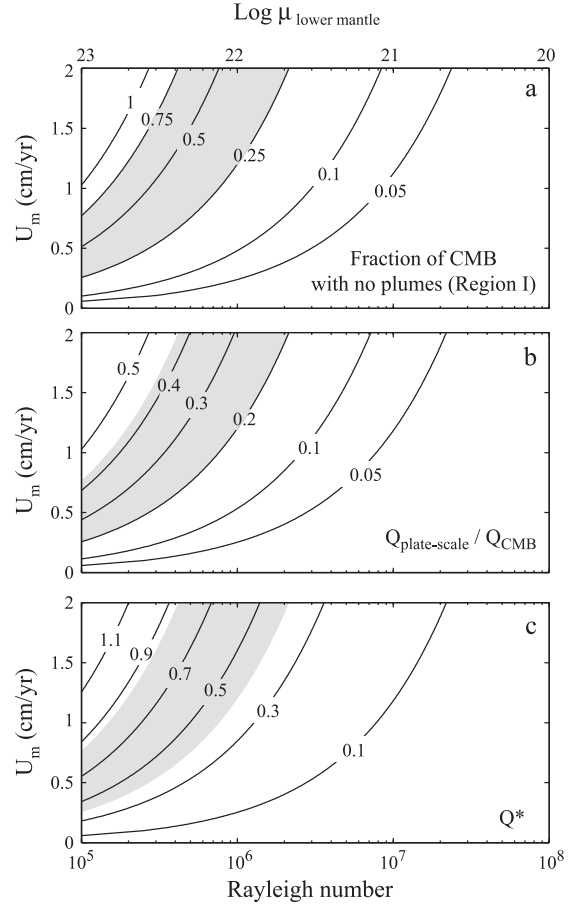

Fig. 8. (a) Fractional area of CMB over which plumes are suppressed (Region I). Assumes a width of downwelling flow (perpendicular to the flow direction, x) of one half the circumference of the CMB. The shaded area, based on the distribution of hotspots at the Earth's surface, is the most likely range of U and Ra (or equivalent $\mu_{lower\ mantle}$) applicable to the Earth's lowermost mantle. (b) Fraction of total CMB heat flow due to plate-scale flow. (c) Magnitude of heat-flux heterogeneity, Q^*. For $Q^* \geq 0.7$, Sumita and Olson [22] find a distinct flow regime (global locking) for convective flow in a rapidly rotating hemispherical shell. Based on the assumptions and results shown in (a), thermal convection in the Earth's outer core falls near the threshold $Q^* = 0.7$ (shaded area).

which appear to be concentrated toward spreading ridges and away from subduction zones. Hotspots, though somewhat dependent on the specific selection criteria, appear to be strongly correlated with regions of slow seismic velocities in the lowermost mantle [55,57], which in turn appear to be associated with broad zones of converging plate-scale flow

(Fig. 7), i.e., the African and Pacific 'superplumes' [58–63]. Because of the significant flux of hot fluid associated with Region IV, the spatially averaged temperature within Region IV should be high relative to Region III. The same appears to be true within Earth's mantle, as suggested from seismic studies [61], although chemical heterogeneity may be an additional factor in decreasing seismic velocities of these 'warm' areas, e.g., [64,48], and references therein.

6.3. Fraction of core heat flow due to plate-scale flow

Generation of Earth's magnetic field by a core dynamo requires heat flow across the CMB. Estimates of present-day core energetics suggest that core heat flow is near-adiabatic [14,65–67]. Inferred ages of the Earth's inner core range between approximately 3.5 and <1 Gy [14,68–70] and are critically sensitive to assumptions in core heat flow throughout Earth's history.

Fig. 8b shows the fraction of core heat that is solely due to plate-scale mantle flow, $Q_{plate-scale}=Q_{CMB}-Q_{Pe=0}$, as a function of Ra and U_m. The shaded area is the likely range of parameters applicable to the Earth (see Fig. 8a). It is estimated that approximately 30% ($\pm10\%$) of the present-day core heat flow is attributable to plate-scale mantle flow. Changes in plate motions (and presumably U_m) of 50% could result in a change in core heat flow of approximately 10%. If core heat flow is near-adiabatic and changes in plate-tectonic geometry, subduction rates, or plate avalanches, e.g., [71], are indeed able to affect U_m significantly, then the associated changes in core heat flow may have interesting implications for the history of Earth's core and geodynamo.

6.4. Spatial variability in CMB heat flux

Time scales for mantle flow are of order 10–100 My and are expected to induce long-term lateral variability in CMB heat flux due to variations in TBL thickness [12,14]. As a consequence, the core is expected to be dynamically modulated by the overlying mantle [15,19,72–75]. Accordingly, lateral variations in CMB heat flux, based on lower-mantle seismic heterogeneity, have been inferred for numerical geodynamo models [17–19].

To evaluate the average spatial variability in CMB heat flux, we use Eqs. (7) and (8) to calculate the average heat-flux ratio for Region I (i.e., the ratio of spatially averaged heat flux from Region I, $\bar{q}_I$, to heat flux, q_c, at $Pe=0$)

$$\frac{\bar{q}_I}{q_c} = \frac{1}{D} \int\limits_{x=0}^{D} \frac{q(x)}{q_c} \, dx \sim 2C(HPe/D)^{1/2} Ra^{-\beta} = 2. \quad (10)$$

Thus, on average CMB heat flux varies by approximately a factor of 2, consistent with a lateral temperature variation in the lowermost mantle of approximately ±500 K [22], with areas of high and low heat flux each extending over approximately 50% of the CMB (based on observed hotspot distribution). Recent experimental work [20,22] has demonstrated that the convective flow pattern in a rotating spherical shell can be modulated by heat-flux heterogeneities at the outer boundary, implying that heterogeneous CMB heat flux may alter the convective flow throughout large parts of the outer core [19], or affect the potential density stratification of the outer core [21]. Independently, it has been suggested that spatially heterogeneous CMB heat-flux is important in terms of long-period trends in paleomagnetic data such as: (1) gradual changes in average reversal frequency over periods of 10^8 years [76]; (2) stationary non-dipole features in the magnetic field [16,17,77]; (3) paleosecular variations in the geomagnetic field [16,78–80]; (4) correlations between time-averaged paleomagnetic inclinations and global plate-tectonic geometry during the Mesozoic and Paleozoic eras [18,77]; (5) modulated reversal frequency in numerical dynamo calculations with variable CMB heat flux [17,81]; and (6) longitudinal variation in inner-core seismic structure [22,82].

Sumita and Olson [22] find a significant change in the convective pattern of a rapidly rotating hemispherical shell when the ratio of applied spatial heat flow heterogeneity at its outer boundary to the total heat flow, Q^*, reaches a value of approximately 0.7. They define this as 'global locking'. When applied to the Earth's outer core, $Q^*=0.7$ should be regarded as an upper limit for global locking (section 6.1 of [22]). Under the assumptions stated in Section 6.1, it is possible to estimate the magnitude of heat-flux

heterogeneity associated with the CMB in an equivalent manner to [22] as

$$Q^* = \frac{\text{Total heat flow Region I}}{\text{Total heat flow } CMB}$$

$$= \left(1 + \frac{A_{II}}{A_I} \frac{q_c}{\bar{q}_I}\right)^{-1}, \tag{11}$$

where $A_{II} = R_{core} - D$ is the estimated areal extent of Region II along the CMB (see also Fig. 8a). The value of Q^*, as a function of Ra and U, is shown in Fig. 8c. Interestingly, we find that for the Earth's core $Q^* \approx 0.7$. This estimate implies that the thermally convective flow pattern in the Earth's outer core could potentially be modulated by spatial heterogeneity in CMB heat flux associated with plate-scale mantle flow. However, a few words of caution are warranted. The experiments of Sumita and Olson do not account for the effect of magnetic forces and stable stratification [15] or the effect of compositional convection. Furthermore, is it not clear to what extent the threshold $Q^* \geq 0.7$ applies to heat-flux heterogeneities extending over 25% or more of the CMB (Sumita, personal communication). Nonetheless, under most conditions, changes in the geometry of heat-flux heterogeneity (at $Q^* > 0.7$) appear to affect the convective flow pattern in Sumita and Olson's experiments (section 3.1.6 of [22]). Therefore, it is feasible that the convective flow in the Earth's outer core (and presumably the geodynamo) is sensitive to changes in heat flux at the CMB caused by variations in plate-scale mantle flow throughout Earth's history.

7. Concluding remarks

The main results of our study are contained in Fig. 6, where we show that a simple boundary layer scaling theory explains satisfactorily the effects of large-scale flow on a hot, low viscosity boundary layer and on plume instabilities arising from that boundary layer. The experiments also illustrate that the subdivision of qualitative behavior into Regions I–IV provides a reasonable conceptual framework for interpreting the effects of large-scale flow on plumes. Our experiments suffer the shortcoming that downwellings are not driven by sinking of the upper

boundary layer, so numerical simulations are probably required in order to extend our results to more realistic circumstances. Nevertheless, brief consideration of the potential applications to mantle plumes and the dynamical regime of the CMB, as outlined in the previous section, suggests that much insight, as well as quantitative predictions, are available through a combination of straightforward boundary layer theory and experimental measurements.

Application of our experimental results (Eqs. (7) and (8)) to the Earth's CMB suggest that plate-scale mantle flow can locally thin the TBL and suppress plume formation over large fractions of the CMB. Assuming that plumes are suppressed over approximately 50% of the CMB (based on the observed distribution of hotspots), we conclude that heat flow from the core is approximately $30 \pm 10\%$ higher than it would be in the absence of plate-scale flow. Furthermore, CMB heat flux is non-uniformly distributed along the CMB, with the spatially averaged heat flux varying by approximately a factor of 2. Application of Sumita and Olson's scaling for heat-flux heterogeneity [22] to our results suggests that the convective flow pattern of the Earth's outer core may be relatively sensitive to changes in the spatially heterogeneous heat flux across the CMB. Hence, changes in plate-scale mantle flow associated with changes in plate-tectonic geometry, subduction rates, or plate avalanches [71] may significantly affect the dynamics of the Earth's outer core and hence the geodynamo. Finally, as a consequence of plume suppression and 'focusing' of hot mantle from the CMB into regions of lower-mantle upwelling, plume conduits (hotspots) are expected to be spatially associated with observed zones of slow seismic velocities, inferred to be zones of hot mantle upwelling flow [61].

References

[1] S. Labrosse, Hotspots, mantle plumes and core heat loss, Earth Planet. Sci. Lett. 199 (2002) 147–156.

[2] G.F. Davies, Ocean bathymetry and mantle convection: 1. Large-scale flow and hotspots, J. Geophys. Res. 93 (1988) 10467–10480.

[3] N.H. Sleep, Hotspots and mantle plumes—some phenomenology, J. Geophys. Res. 95 (1990) 6715–6736.

[4] M.A. Richards, D.C. Engebretson, Large-scale mantle convection and the history of subduction, Nature 355 (1992) 437–440.

[5] M.A. Richards, R.W. Griffiths, Deflection of plumes by mantle shearflow—experimental results and a simple theory, Geophys. J. 94 (1988) 367–376.

[6] R.W. Griffiths, M.A. Richards, The adjustment of mantle plumes to changes in plate motion, Geophys. Res. Lett. 16 (1989) 437–440.

[7] R.W. Griffiths, I.H. Campbell, On the dynamics of long-lived plume conduits in the convecting mantle, Earth Planet. Sci. Lett. 103 (1991) 214–227.

[8] B. Steinberger, R.J. O'Connell, Advection of plumes in mantle flow: implications for hotspot motion, mantle viscosity, and plume distribution, Geophys. J. Int. 132 (1998) 412–434.

[9] B. Steinberger, Plumes in a convection mantle: models and observations for individual hotspots, J. Geophys. Res. 105 (2000) 11127–11152.

[10] B. Steinberger, R. Sutherland, R.J. O'Connell, Prediction of Emperor-Hawaii seamount locations from a revised model of global plate motion and mantle flow, Nature 430 (2004) 167–173.

[11] E. Tan, M. Gurnis, L.J. Han, Slabs in the lower mantle and their modulation of plume formation, Geochem. Geophys. Geosyst. (2002) 1067.

[12] A.M. Jellinek, H.M. Gonnermann, M.A. Richards, Plume capture by divergent plate motions: implications for the distribution of hotspots, geochemistry of mid-ocean ridge basalts, and estimates of the heat flux at the core–mantle boundary, Earth Planet. Sci. Lett. 205 (2003) 361–378.

[13] B. Buffett, On the thermal evolution of the Earth's core, J. Geophys. Res. 101 (1996) 7989–8006.

[14] B.A. Buffett, Earth's core and the geodynamo, Science 288 (2000) 2007–2012.

[15] J.R. Lister, Thermal winds forced by inhomogeneous boundary conditions in rotating, stratified, hydromagnetic fluid, J. Fluid Mech. 505 (2004) 163–178.

[16] C.L. Johnson, C.G. Constable, The time-averaged geomagnetic field: global and regional biases for 0–5 Ma, Geophys. J. Int. 131 (1997) 643–666.

[17] G.A. Glatzmaier, R. Coe, L. Hongre, P.H. Roberts, The role of the Earth's mantle in controlling the frequency of geomagnetic reversals, Nature 401 (1999) 885–890.

[18] P. Olson, U.R. Christensen, The time-averaged magnetic field in numerical dynamos with non-uniform boundary heat flow, Geophys. J. Int. 151 (2002) 808–823.

[19] S.J. Gibbons, D. Gubbins, Convection in the Earth's core driven by lateral variations in the core–mantle boundary heat flux, Geophys. J. Int. 142 (2000) 631–642.

[20] I. Sumita, P. Olson, A laboratory model for convection in Earth's core driven by a thermally heterogeneous mantle, Science 286 (1999) 1547–1549.

[21] M.G. Wells, R.W. Griffiths, J.S. Turner, Competition between distributed and localized buoyancy fluxes in a confined volume, J. Fluid Mech. 391 (1999) 319–336.

[22] I. Sumita, P. Olson, Rotating thermal convection experiments in a hemispherical shell with heterogeneous boundary heat flux: implications for the Earth's core, J. Geophys. Res. 107 (2002) DOI:10.1029/2001JB000548.

[23] S. Zhong, M. Zuber, L. Moresi, M. Gurnis, Role of temperature-dependent viscosity and surface plates in spherical shell models of mantle convection, J. Geophys. Res. 105 (2000) 11063–11082.

[24] M. Monnereau, S. Quere, Spherical shell models of mantle convection with tectonic plates, Earth Planet. Sci. Lett. 184 (2001) 575–587.

[25] J. Lowman, S. King, C. Gable, Steady plumes in viscously stratified, vigorously convecting, three-dimensional numerical mantle convection models with mobile plates, Geochem. Geophys. Geosyst. 5 (2004) DOI:10.1029/2003GC000583.

[26] J. Niemela, L. Skrbek, K. Sreenivasan, R. Donnelly, Turbulent convection at very high Rayleigh numbers, Nature 404 (2000) 837–840.

[27] M.A. Richards, B.H. Hager, Geoid anomalies in a dynamic Earth, J. Geophys. Res. 89 (1984) 5987–6002.

[28] J.X. Mitrovica, W.R. Peltier, Constraints on mantle viscosity based upon the inversion of postglacial uplift data from the Hudson-Bay region, Geophys. J. Int. 122 (1995) 353–377.

[29] A.M. Forte, J.X. Mitrovica, Deep-mantle high-viscosity flow and thermochemical structure inferred from seismic and geodynamic data, Nature 410 (2001) 1049–1056.

[30] G. Kaufmann, K. Lambeck, Glacial isostatic adjustment and the radial viscosity profile from inverse modeling, J. Geophys. Res. 107 (2002) DOI:10.1029/2001JB000941.

[31] A. Acrivos, J.D. Goddard, Assymptotic expansions for laminar convection heat and mass transfer, J. Fluid Mech. 23 (1965) 273–291.

[32] S. Morris, The effect of a strongly temperature-dependent viscosity on slow flow past a hot sphere, J. Fluid Mech. 124 (1982) 1–26.

[33] S. Morris, D. Canright, A boundary-layer analysis of Benard convection in a fluid of strongly temperature-dependent viscosity, Phys. Earth Planet. Inter. 36 (1984) 355–373.

[34] L.G. Leal, Laminar Flow and Convective Transport Processes, Butterworth-Heinemann, Boston, 1992.

[35] L. Howard, Convection at high Rayleigh number, in: H. Görtler (Ed.), Proc. Elenventh Int. Congress Applied Mechanics, Munich, Springer, Berlin, 1964, pp. 1109–1115.

[36] J. Turner, Buoyancy Effects in Fluids, Cambridge University Press, Cambridge, 1973.

[37] S. Grossmann, D. Lohse, Thermal convection for large Prandtl numbers, Phys. Rev. Lett. 86 (2001) 3316–3319.

[38] F.M. Richter, H. Nataf, S.F. Daly, Heat transfer and horizontally averaged temperature of convection with large viscosity variations, J. Fluid Mech. 129 (1983) 173–192.

[39] E. Giannandrea, U. Christensen, Variable viscosity convection experiments with a stress-free upper boundary and implications for the heat transport in the Earth's mantle, Phys. Earth Planet. Inter. 78 (1993) 139–152.

[40] L. Moresi, V. Solomatov, Numerical investigation of 2D convection with extremely large viscosity variations, Phys. Fluids 7 (1995) 2154–2162.

[41] N. Schaeffer, M. Manga, Interaction of rising and sinking mantle plumes, Geophys. Res. Lett. 28 (2001) 455–458.

[42] J.T. Wilson, A possible origin of the Hawaiian Islands, Can. J. Phys. 41 (1963) 863–870.

[43] W.J. Morgan, Convection plumes in the lower mantle, Nature 230 (1971) 42–43.

[44] M. Stefanick, D.M. Jurdy, The distribution of hot spots, J. Geophys. Res. 89 (1984) 9919–9925.

[45] R.A. Duncan, M.A. Richards, Hotspots, mantle plumes, flood basalts, and true polar wander, Rev. Geophys. 29 (1991) 31–50.

[46] V. Courtillot, A. Davaille, J. Besse, J. Stock, Three distinct types of hotspots in the Earth's mantle, Earth Planet. Sci. Lett. 205 (2003) 295–308.

[47] T. Lay, Q. Williams, E. Garnero, L. Kellogg, M. Wysession (Eds.), Seismic wave anisotropy in the D'' region and its implications, The Core–Mantle Boundary Region, American Geophysical Union, Washington, DC, USA, 1998.

[48] A.M. Jellinek, M. Manga, Links between long-lived hotspots, mantle plumes, D'' and plate tectonics, Geophys. Rev. (in press).

[49] R.D. van der Hilst, S. Widiyantoro, E.R. Engdahl, Evidence for deep mantle circulation from global tomography, Nature 386 (1997) 578–584.

[50] S.P. Grand, Mantle shear-wave tomography and the fate of subducted slabs, Philos. Trans. R. Soc., A 360 (2002) 2475–2491.

[51] G.F. Davies, M.A. Richards, Mantle convection, J. Geol. 100 (1992) 151–206.

[52] A. Lenardic, W.M. Kaula, Tectonic plates, D'' thermal structure, and the nature of mantle plumes, J. Geophys. Res. 99 (1994) 15697–15708.

[53] A.M. Jellinek, A. Lenardic, M. Manga, The influence of interior mantle temperature on the structure of plumes: heads for Venus, tails for the Earth, Geophys. Res. Lett. 29 (2002) DOI:10.1029/2001GL014624.

[54] A. Forte, J. Mitrovica, A. Espesset, Geodynamic and seismic constraints on the thermochemical structure and dynamics of convection in the deep mantle, Philos. Trans. R. Soc., A 360 (2002) 2521–2543.

[55] M.A. Richards, B.H. Hager, N.H. Sleep, Dynamically supported geoid highs over hotspots: observation and theory, J. Geophys. Res. 93 (1988) 7690–7708.

[56] S.A. Weinstein, P.L. Olson, The proximity of hotspots to convergent and divergent plates, Geophys. Res. Lett. 16 (1989) 433–436.

[57] T. Ray, D.L. Anderson, Spherical disharmonics in the Earthsciences and the spatial solution—ridges, hotspots, slabs, geochemistry and tomography correlations, J. Geophys. Res. 99 (1994) 9605–9614.

[58] B.H. Hager, R.W. Clayton, M.A. Richards, R.P. Comer, A.M. Dziewonski, Lower mantle heterogeneity, dynamic topography, and the geoid, Nature 313 (1985) 541–545.

[59] A. Dziewonski, J. Woodhouse, Global images of the Earth's interior, Science 236 (1987) 37–48.

[60] M. McNutt, Superswells, Rev. Geophys. 36 (1998) 211–244.

[61] B. Romanowicz, Y.C. Gung, Superplumes from the core–mantle boundary to the lithosphere: implications for heat flux, Science 296 (2002) 513–516.

[62] B. Romanowicz, 3D structure of the Earth's lower mantle, C. R. Geosci. 335 (2003) 23–35.

[63] M. Panning, B. Romanowicz, Inferences on flow at the base of Earth's mantle based on seismic anisotropy, Science 303 (2004) 351–353.

[64] E.J. Garnero, Heterogeneity of the lowermost mantle, Annu. Rev. Earth Planet. Sci. 28 (2000) 509–537.

[65] B.A. Buffett, Estimates of heat flow in the deep mantle based on the power requirements for the geodynamo, Geophys. Res. Lett. 29 (2002) DOI:10.1029/2001GL014649.

[66] J.R. Lister, B.A. Buffett, The strength and efficiency of thermal and compositional convection in the geodynamo, Phys. Earth Planet. Inter. 91 (1995) 17–30.

[67] U. Christensen, A. Tilgner, Power requirement of the geodynamo from ohmic losses in numerical and laboratory dynamos, Nature 429 (2004) 169–171.

[68] S. Labrosse, J.P. Poirier, J.L. Le Mouel, The age of the inner core, Earth Planet. Sci. Lett. 190 (2001) 111–123.

[69] A. Brandon, R. Walker, I. Puchtel, H. Becker, M. Hymayun, S. Revillon, Os-186–Os-187 systematics of Gorgona Island komatiites: implications for early growth of the inner core, Earth Planet. Sci. Lett. 206 (2003) 411–426.

[70] D. Gubbins, D. Alfe, G. Masters, G. Price, M. Gillan, Can the Earth's dynamo run on heat alone? Geophys. J. Int. 155 (2003) 609–622.

[71] S.A. Weinstein, Catastrophic overturn of the earth's mantle driven by multiple phase changes and internal heat generation, Geophys. Res. Lett. 20 (1993) 101–104.

[72] G. Jones, Thermal interaction of the core and the mantle and long-term behavior of the geomagnetic field, J. Geophys. Res. 82 (1977) 1703–1709.

[73] D. Gubbins, M. Richards, Coupling of the core dynamo and mantle—thermal or topographic? Geophys. Res. Lett. 13 (1986) 1521–1524.

[74] J. Bloxham, D. Gubbins, Morphology of the geomagnetic field and implications for the geodynamo, Nature 325 (1987) 509–511.

[75] J. Bloxham, A. Jackson, Lateral temperature-variations at the core–mantle boundary deduced from the magnetic-field, Geophys. Res. Lett. 17 (1990) 1997–2000.

[76] A. Cox, Frequency of geomagnetic reversals and symmetry of nondipole field, Rev. Geophys. 13 (1975) 35–51.

[77] J. Bloxham, The effect of thermal core–mantle interactions on the 33 palaeomagnetic secular variation, Philos. Trans. R. Soc., A 358 (2000) 1171–1179.

[78] J. Bloxham, D. Gubbins, A. Jackson, Geomagnetic secular variation, Philos. Trans. R. Soc., A 329 (1989) 415–502.

[79] D. Gubbins, P. Kelly, Persistent patterns in the geomagnetic-field over the past 2.5 Myr, Nature 365 (1993) 829–832.

[80] J. Bloxham, Time-independent and time-dependent behaviour of high-latitude flux bundles at the core–mantle boundary, Geophys. Res. Lett. 29 (2002) DOI:10.1029/2001GL014543.

[81] U.R. Christensen, P. Olson, Secular variation in numerical geodynamo models with lateral variations of boundary heat flow, Phys. Earth Planet. Inter. 138 (2003) 39–54.

[82] S.N. Luo, S.D. Ni, D. Helmberger, Relationship of D'' structure with the velocity variations near the inner-core boundary, Geophys. Res. Lett. 29 (2002) DOI:10.1029/2001GL013907.